JCB Article

Mice with targeted disruption of the fatty acid transport protein 4 (Fatp 4, Slc27a4) gene show features of lethal restrictive dermopathy

Thomas Herrmann,[1] Frank van der Hoeven,[2] Hermann-Josef Gröne,[3] Adrian Francis Stewart,[5] Lutz Langbein,[4] Iris Kaiser,[1] Gerhard Liebisch,[6] Isabella Gosch,[1] Florian Buchkremer,[1] Wolfgang Drobnik,[6] Gerd Schmitz,[6] and Wolfgang Stremmel[1]

[1]Department of Internal Medicine IV, University of Heidelberg, 69115 Heidelberg, Germany
[2]Transgenic Core Facility, [3]Department of Cellular and Molecular Pathology, and [4]Department of Cell Biology, German Cancer Research Center, 69120 Heidelberg, Germany
[5]Biotec, Technical University of Dresden, 01307 Dresden, Germany
[6]Institute of Clinical Chemistry, University of Regensburg, 93042 Regensburg, Germany

The fatty acid transport protein family is a group of evolutionarily conserved proteins that are involved in the cellular uptake and metabolism of long and very long chain fatty acids. However, little is known about their respective physiological roles. To analyze the functional significance of fatty acid transport protein 4 (Fatp4, Slc27a4), we generated mice with a targeted disruption of the *Fatp4* gene. *Fatp4*-null mice displayed features of a neonatally lethal restrictive dermopathy. Their skin was characterized by hyperproliferative hyperkeratosis with a disturbed epidermal barrier, a flat dermal–epidermal junction, a reduced number of pilo-sebaceous structures, and a compact dermis. The rigid skin consistency resulted in an altered body shape with facial dysmorphia, generalized joint flexion contractures, and impaired movement including suckling and breathing deficiencies. Lipid analysis demonstrated a disturbed fatty acid composition of epidermal ceramides, in particular a decrease in the C26:0 and C26:0-OH fatty acid substitutes. These findings reveal a previously unknown, essential function of Fatp4 in the formation of the epidermal barrier.

Introduction

The mechanism of cellular fatty acid uptake has so far remained poorly understood. The passive diffusion theory is counterparted by the concept of a carrier-mediated uptake process. It presently appears that both pathways may operate in conjunction with one another in a complex lipid transport mechanism involving both extra- and intracellular acceptor molecules (Stremmel et al., 2001).

The family of fatty acid transport proteins (Fatp)* is of particular interest in the overall process of cellular fatty acid uptake. The first member was identified as part of an expression screen for the cellular enrichment of a fluorescent long chain fatty acid analogue (Schaffer and Lodish, 1994). Two proteins were identified, one of which was the murine homologue of the known rat long chain fatty acid acyl-CoA synthetase, and the other a previously unknown component, and thus referred to as Fatp. Fatty acid uptake studies with cultured murine 3T3-L1 cells stably transfected with *Fatp* have revealed a three- to fourfold increase in [^{14}C]oleic acid uptake when compared with control cells (Schaffer and Lodish, 1994). To date, six members of this family have been described (Hirsch et al., 1998; Gimeno et al., 2003).

A detailed analysis of the membrane topology of Fatp1 has revealed one transmembrane domain and multiple membrane-associated domains peripherally associated with the inner leaflet of the plasma membrane (Lewis et al., 2001). There are two large stretches of nonmembrane-associated amino

Address correspondence to Wolfgang Stremmel, Dept. of Internal Medicine IV, University of Heidelberg, Bergheimer Str. 58, 69115 Heidelberg, Germany. Tel.: 49-62-21-56-87-00. Fax: 49-62-21-56-41-16. E-mail: wolfgang_stremmel@med.uni-heidelberg.de

*Abbreviations used in this paper: CER, ceramide; ESI-MS/MS, electrospray ionization tandem mass spectrometry; Fatp, fatty acid transport protein; FC, cholesterol; PC, phosphatidylcholine; PE, phosphatidylethanolamine; PS, phosphatidylserine; SPM, sphingomyelin; TEWL, transepidermal water loss; X-gal, 5-bromo-4-chloro-3-indolyl-β-D-galactopyranoside.

Key words: ceramides; epidermis; Fatp4; fatty acid metabolism; fatty acid transport

acid residues oriented toward the cytosol, one of them carrying a highly conserved AMP-binding motif. Only a very short segment of the amino terminus faces the extracellular side of the membrane bilayer.

Specific binding sites for fatty acids within the Fatp structure have not yet been identified. Several reports have demonstrated acyl-CoA synthetase activity of Fatp1, 2, 4, and 5 for various lipid compounds, fatty acids in particular; of special interest here is the preference for the activation of very long chain fatty acids, as demonstrated for Fatp1, 2, and 4 (Berger et al., 1998; Coe et al., 1999; Steinberg et al., 1999; Herrmann et al., 2001). How the activation to acyl-CoA is related to cellular fatty acid uptake is currently unclear. Because it has been identified as the major intestinal Fatp and localized to the apical side of enterocytes (Stahl et al., 1999), we have focused our interest on Fatp4. In previous works, we detected *Fatp4* mRNA in the small intestine, brain, kidney, liver, skin, and heart (Herrmann et al., 2001).

To evaluate the impact of Fatp4 on fatty acid transport, Stahl et al. (1999) performed *Fatp4*-targeted antisense oligonucleotide experiments in isolated enterocytes and could verify a 50% inhibition of oleate and palmitate uptake after incubation with *Fatp4* antisense oligonucleotides. To further elucidate the physiological role of this protein in the complex mammalian organism, we have generated a mouse line with a targeted *Fatp4* disruption. Examination of the resulting phenotype has revealed an unexpected essential role of Fatp4 in the epidermis.

Results

Generation of *Fatp4* mutant mice

The targeting strategy used for the generation of *Fatp4* mutant mice is shown in Fig. 1 A. A gene trap vector was integrated into intron 2 of the *Fatp4* gene. The targeting vector included a 7172-bp cassette containing a splice acceptor (SA), an internal ribosome entry site (IRES), a *lacZ* reporter gene, a neomycin resistance gene, and a poly(A)$^+$ signal to terminate the transcription. To enable the subsequent generation of conditional *Fatp4* −/− mice, this cassette was flanked by FLP recombinase target (FRT) sites, followed by loxP sites on either side of exon 3.

Southern blot and PCR analysis were used to identify homologous recombinants and to follow the *Fatp4* mutant alleles during the generation of the two mouse lines F12K and F13K derived from two separate embryonic stem cell clones (Fig. 1, B and C). Northern blot analysis revealed strong *Fatp4* mRNA expression in Fatp4 +/+ intestine, whereas *Fatp4* mRNA in *Fatp4* −/− intestine could not be detected, indicating a severe loss-of-function allele of *Fatp4* (Fig. 1 D). Using Western blot analyses, we detected Fatp4 in liver (not depicted), intestine (Fig. 1 E), and skin (Fig. 1 F) of *Fatp4* +/+ mice, whereas in the same organs of *Fatp4* −/− mice no Fatp4-specific signal was obtained.

As the mutant allele *Fatp4-K* was generated by integrating a gene trap vector into the *Fatp4* gene, it would principally be conceivable that this mutant *Fatp4* allele might not be a null, but rather a hypomorphic allele. Thus, as a control, we generated another mutant allele (which we referred to as *Fatp4-KO*) by crossing mice carrying the *Fatp4-K* allele with

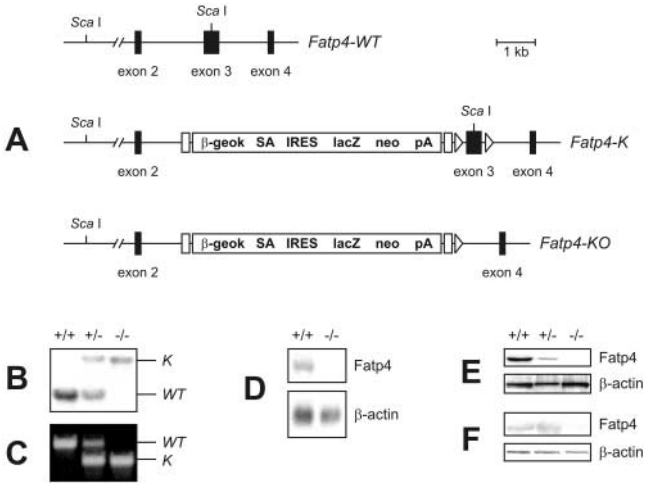

Figure 1. ***Fatp4* knockout strategy, genotype analysis, and verification of absent *Fatp4* expression in *Fatp4* −/− mice.** (A) *Fatp4* locus before (wild-type, *Fatp-WT*) and after (mutant allele, *Fatp-K*) homologous recombination with the targeting vector insert. Cre recombinase converts the allele *Fatp4-K* to the allele *Fatp4-KO,* which lacks exon 3. LoxP sites are depicted as open triangles, FRT sites as open rectangles. (B) Southern analysis of the *Fatp4* locus. *Fatp4* +/+, +/−, and −/− DNA was digested with ScaI, subjected to gel electrophoresis, and transferred to a nylon membrane. The filter was hybridized with a *Fatp4* 5′ probe, washed, and exposed to film. (C) PCR genotype analysis of tail DNA. An ethidium bromide–stained agarose gel containing amplification products from *Fatp4* +/+, +/−, and −/− mice is shown. The primer combination mmF4-In2f/mmF4-pUX4r detects the mutant allele (K), the primer combination mmF4-In2f/mmF4-wtIn3r the wild-type allele (WT). (D) Northern blot analysis of *Fatp4* +/+ and Fatp4 −/− RNA from total intestine using a specific *Fatp4* cDNA probe and a β-actin control probe, respectively. The respective probe is noted on the right, the genotype is marked above the lanes. (E and F) Immunoblot of Fatp4 and β-actin in total intestine (E) and skin (F) homogenates. Tissue homogenates were prepared from *Fatp4* +/+, *Fatp4* +/−, and *Fatp4* −/− mice, subjected to SDS/PAGE, and blotted. The respective antibody is noted on the right, the genotype is marked above the lanes. The Fatp4 peptide sequence recognized by the antibody is APKHLPSHPDKGFTD (aa 225–239 of the Fatp4 protein), which is encoded by a nucleotide sequence in exons 4 and 5. The data are representative of three separate experiments.

mice transgenic for PGK-Cre (Schwenk et al., 1995). The *Fatp4-KO* allele retained the gene trap cassette but lacked the exon 3 of the *Fatp4* gene (Fig. 1 A). If splicing around the gene trap cassette occurred, the *Fatp4* allele lacking exon 3 would result in the formation of a stop codon at nucleotide position 169–171, rendering the synthesis of a functional Fatp4 protein impossible. Analysis of neonatal mice homozygous for the *Fatp4-KO* allele revealed morphological features identical to those observed in homozygous *Fatp4-K* mice, thus indicating that the *Fatp4-K* allele was a null allele and that the gene trap cassette was highly effective.

Phenotype of *Fatp4* mutant mice

Fatp4 heterozygous mice were phenotypically indistinguishable from wild-type mice and reproduced normally. In contrast, *Fatp4* −/− mice died shortly (minutes to a few hours) after birth. Genotype analysis of 260 newborns from 31 intercrosses demonstrated that the frequencies of born wild-type, heterozygous, and mutant homozygous mice were

Table I. **Numbers and body weights of newborn *Fatp4* +/+, *Fatp4* +/−, and *Fatp4* −/− mice**

Genotype	Number of newborn mice	Mean body weight ± SD
		(g)
Fatp4 +/+	63 (24.2%)	1.37 ± 0.14
Fatp4 +/−	131 (50.4%)	1.40 ± 0.14
Fatp4 −/−	66 (25.4%)	1.25 ± 0.15***

***, $P < 0.001$.

Mendelian (Table I). These results demonstrate that there is no pronounced embryonic or fetal lethal phenotype associated with the *Fatp4* mutant allele. No phenotypical differences of *Fatp4* −/− mice were observed before embryonic day 16.5. As heterozygotes appear indistinguishable from wild-type littermates, the insertion of additional sequences from the targeting construct at the *Fatp4* locus is apparently not associated with a dominant phenotype.

At birth, *Fatp4* −/− progeny revealed a significantly lower body weight (Table I) and had a markedly abnormal appearance with facial dysmorphia and a compressed, rigid torso with thickened skin extending over and covering the proximal extremities, the joints of which were fixed in flexion contracture (Fig. 2, A–C). The skin layer appeared to be too small for size of the body. This disproportion between the body content and the surrounding skin led to a characteristic protrusion of the tongue in all neonatal *Fatp4* −/− mice and to an abdominal hernia with intestinal protrusion in 16% of the animals. Due to the remarkable appearance of the *Fatp4* −/− pups when compared with heterozygous and wild-type littermates, their skeletons were fixed and examined after staining with Alcian blue and Alizarin red S. However, no significant anomalies of either cartilage or bones were observed (Fig. 2 D). At birth, the skin of *Fatp4* −/− mice appeared thickened and exhibited a taut, scaly, wrinkle-free surface with an overall waxy appearance. Within this rigid armor of skin, body movements of the pups were highly restricted; they could move only very slowly and were not able to breathe or suckle normally.

The stratum corneum of the *Fatp4* −/− progeny was considerably thicker than that of normal epidermis. In contrast to the multilayer stratum corneum of wild-type mice, the corneal layer of the null variant appeared as a hyperkeratotic, homogeneous, eosinophilic mass. The corneal layers appeared to be plastered together and failed to shed. The stratum granulosum demonstrated significantly smaller keratohyalin granules. Finally, the stratum spinosum was characterized by an increased number of cell layers, and the dermo–epidermal junction was flat and showed a lack of rete pegs (Fig. 3 A). In comparison with the dermis of *Fatp4* +/+ control littermates, the dermis of *Fatp4* −/− mice appeared condensed with compact collagen fibers (Fig. 3 B). The pilosebaceous structures were significantly reduced in number and appeared less developed (not depicted). No significant difference in regard to the fatty tissue in the hypodermis could be detected between *Fatp4* −/− mice and wild-type littermates.

EM confirmed the light microscopic findings, in particular, the significantly smaller size of the keratohyalin granules

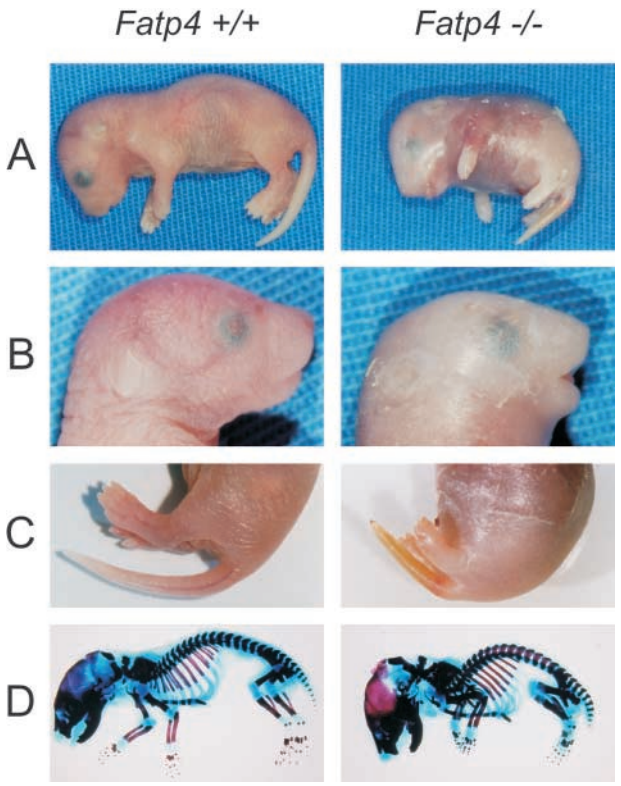

Figure 2. **Gross analyses of newborn *Fatp4* −/− mice and *Fatp4* +/+ control littermates.** (A–C) Gross morphology of *Fatp4* mutant neonates. At birth, *Fatp4* −/− progeny were smaller and had a markedly abnormal appearance with facial dysmorphia, a compressed torso, and a taut skin exhibiting a scaly, wrinkle-free surface and extending over and covering the proximal extremities, the joints of which were fixed in flexion contracture. (D) Alcian blue/Alizarin red S staining of wild-type and homozygous mutant skeletons revealed no gross morphological differences, neither in bone nor in cartilage. The flexion joint contractures persisted after the staining procedure.

in the stratum granulosum of *Fatp4* −/− pups (Fig. 3 C). The intercellular junctions appeared equally distributed within the stratum spinosum of *Fatp4* +/+ and *Fatp4* −/− pups. Using ruthenium tetroxide reaction, lamellar bodies could be detected in the epidermis of both *Fatp4* +/+ and *Fatp4* −/− mice (not depicted), but a detailed morphometric analysis was not performed.

The structural changes described pointed to a metabolic defect originating from within the skin itself. Although in previous papers the presence of *Fatp4* mRNA in skin was demonstrated (Herrmann et al., 2001), it was unclear in which cell layer the protein was synthesized. Therefore, we generated antibodies specific for Fatp4 and performed immunofluorescence microscopy of skin samples of wild-type and *Fatp4* −/− mice. With the "standard" protocol, for optimal penetration, using Triton X-100 as detergent and prolonged application and washing times (see Materials and methods), the stratum granulosum showed an intense granular immunostaining in *Fatp4* +/+ mice, whereas in *Fatp4* −/− mice, only an extremely fine and faint granular staining was detected (unpublished data). As the significance of this reaction after a somewhat destructive detergent treatment was not clear, we used alternative protocols designed to mini-

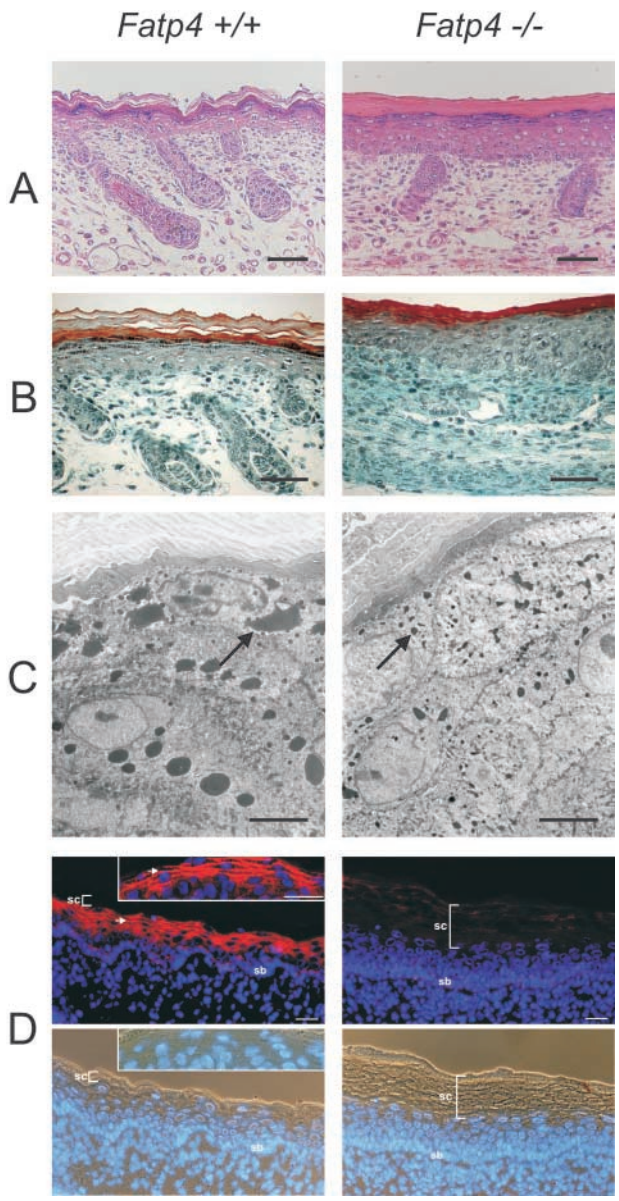

Figure 3. **Skin of newborn *Fatp4* −/− mice and *Fatp4* +/+ control littermates.** (A) Neonatal dorsal skin stained with hematoxylin and eosin. In comparison with control epidermis, *Fatp4* −/− epidermis exhibits an increased number of cell layers in the stratum spinosum and the basal layer, significantly smaller granula in the stratum granulosum, and a compact, thickened stratum corneum. Bars, 50 μm. (B) Neonatal snout skin stained with Masson's trichrome. In comparison with wild-type dermis, the dermis of Fatp4 −/− mice appears condensed with more compact collagen fibers. Bars, 50 μm. (C) Ultrastructural analysis of epidermis of *Fatp4* −/− mice and wild-type littermates (osmium tetroxide fixation). In comparison with control epidermis, the epidermis of *Fatp4* −/− mice is characterized by significantly smaller, often irregularly shaped granules (arrow) in the stratum granulosum. Bars, 5 μm. (D, top) In *Fatp4* +/+ mice, immunostaining using Fatp4 antiserum shows prominent staining along the cell–cell borders (arrows) in upper layers of the stratum spinosum and in the stratum granulosum subjacent to the stratum corneum (sc), besides a very faint and sparse staining in the lower layers of the stratum spinosum. The inset shows a higher magnification. In *Fatp4* −/− mice, these structures appear negative for such a staining pattern. Only a very faint staining is detectable in cells of the stratum basale (sb) of both wild-type and *Fatp4* −/− mice. (Bottom) Phase-contrast images of the same sections. Blue: DAPI nuclear staining. Bars, 50 μm.

mize losses of membrane material and small cytoplasmic proteins. Remarkably, when using procedures without detergent addition in any of the fixation and incubation steps (see Materials and methods), a prominent and specific antibody decoration along the cell borders of the upper layers of the stratum spinosum and the entire stratum granulosum was seen in wild-type mice (Fig. 3 D and insert therein; arrows), and a relatively faint cytoplasmic staining was seen in the keratinocytes of the lower stratum spinosum. Both reactions were markedly reduced in peptide competition experiments (unpublished data). All other controls (see Materials and methods) were negative, except for a faint staining in the basal cell layer that was also detectable in the *Fatp4* −/− mice (Fig. 3 D), and thus probably due to a nonspecific reaction.

As the skin of the Fatp4-deficient mice showed a hyperplastic, hyperkeratotic, and parakeratotic appearance, we investigated the stage of differentiation of keratinocytes, particularly the distribution of specific keratins and of proteins of the cornified envelope. Keratins K5 (unpublished data) and K 14 (Fig. 4 A) were restricted to the stratum basale of wild-type skin. The skin of the *Fatp4* −/− mice showed a comparable immunostaining pattern but with an extension of the labeling to the first suprabasal cells (Fig. 4 A, open arrow), indicative for an enhanced cell proliferation in the *Fatp4* −/− skin. A strong keratin K10 staining could be observed in all living suprabasal cell layers (Fig. 4 B), but appeared much broader in the *Fatp4* −/− mice. Both the stratum basale and the stratum corneum remained unstained in both kinds of mice. The immunostaining of keratin K2e was restricted to only a few cells (unpublished data). The clear proliferative and reactive character of the *Fatp4* −/− epidermis was also demonstrable by the intense reaction of keratins K6 (Fig. 4 C) and K16 (unpublished data): Although the epidermis of the *Fatp4* +/+ mice was clearly negative for both keratins, both K6 and K16 were labeled in *Fatp4* −/− mouse cells in the suprabasal layers, the stratum spinosum, and in particular, stratum granulosum, including the cornified cells of the stratum corneum. Furthermore, the stage of cornification of the skin keratinocytes was investigated by the immunolocalization of loricrin (Fig. 4 D), filaggrin, periplakin, and transglutaminase 1 (unpublished data). All of these proteins were seen in their typical localizations in both the wild-type and the mutant animals, with the only consistent difference being that the number of cell layers showing immunostaining was higher in the skin of *Fatp4* −/− mice, indicative of hyperkeratinization. Immunohistochemical staining of the tight junction proteins occludin, claudin-1, and protein ZO-1 appeared in their typical wild-type localization (compare Morita et al., 1999; Brandner et al., 2002; Langbein et al., 2002), i.e., occludin exclusively in the stratum granulosum, in the *Fatp4* −/− animals sometimes with an additional layer (Fig. 4 E), whereas claudin-1 and protein ZO-1 could also be detected at the cell margins of cells of the lower strata (unpublished data; Morita et al., 1999; Brandner et al., 2002; Langbein et al., 2002).

To examine whether the observed abnormal skin structure might also be associated with an impaired skin barrier function, several techniques were applied. The fluorescent dye Lucifer yellow permeated throughout the entire epidermis in *Fatp4* −/− pups. In contrast, it did not pass through the up-

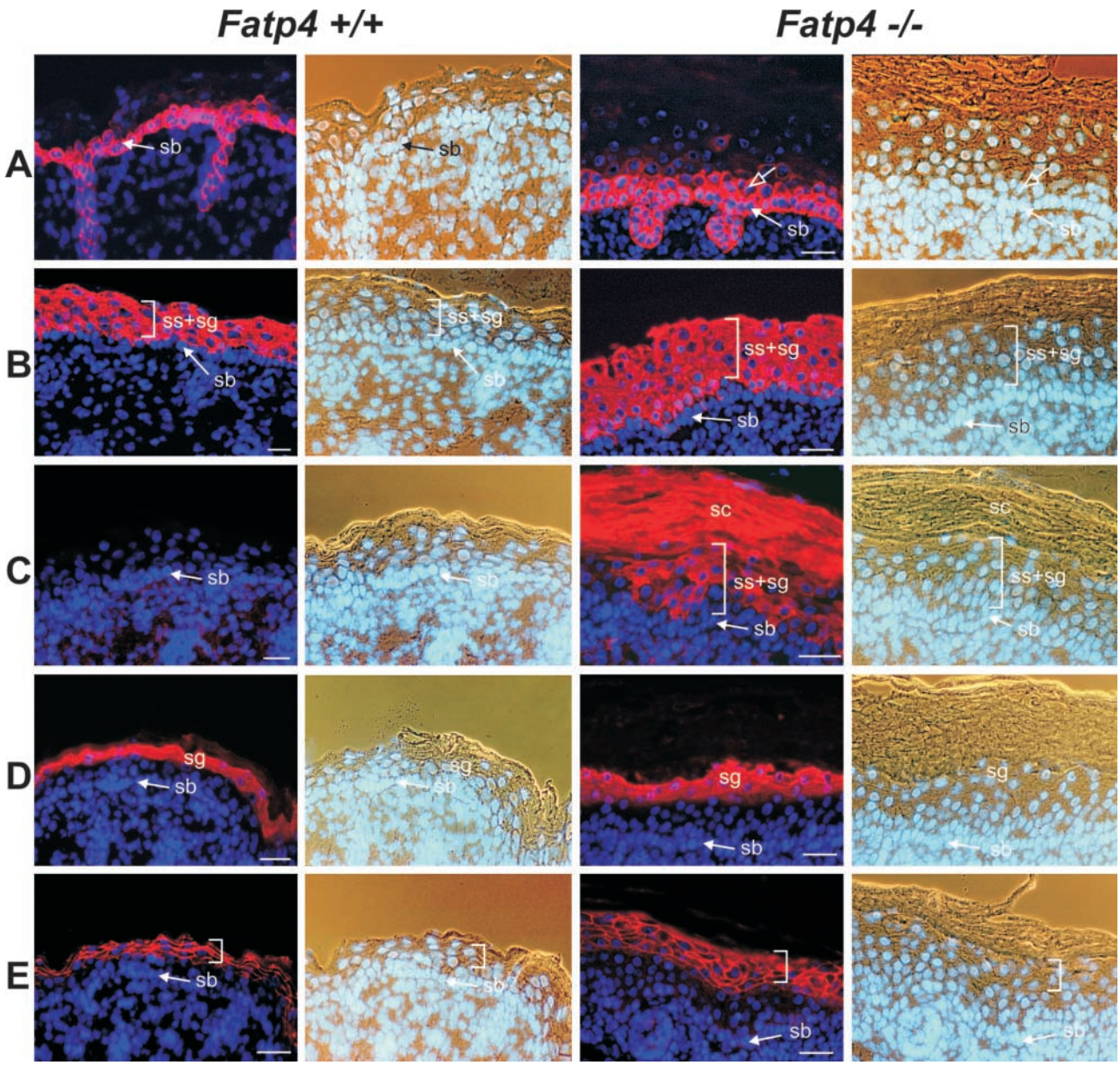

Figure 4. **Differentiation of neonatal skin of newborn *Fatp4* −/− and control *Fatp4* +/+ mice, as shown by immunofluorescence microscopy.** (A) Immunofluorescence microscopy of keratin K14 in dorsal skin. In the *Fatp4* +/+ control mice, K14 is restricted to the stratum basale (sb) and in the *Fatp4* −/− mice is additionally detected in the first layers of the stratum spinosum (open arrow). (B) With keratin K10 antibodies, the stratum spinosum and the stratum granulosum (ss+sg) are strongly stained in both wild-type and *Fatp4* −/− mice. However, note that both layers are thicker in the mutant. (C) Immunostaining of K6 is negative in the *Fatp4* +/+, but intense in the upper suprabasal layers, including the stratum corneum (sc), of the *Fatp4* −/− mice. (D) Loricrin as a typical protein of the cornified envelope is detected in the stratum granulosum (sg) and seems to be a bit more prominent in the mutant mice. (E) The presence of occludin in the plasma membranes of the stratum granulosum (bracket; sb, stratum basale) is seen in a somewhat broader appearing zone in the mutant mice, indicating an intact tight junction barrier in both kinds of mice. To the right of each of the immunofluorescence micrographs are the specific phase-contrast images of the same sections. Blue: DAPI nuclear staining. Bars, 50 μm.

per layers of the stratum corneum in wild-type neonatal mice. (Fig. 5 A). In another set of experiments, it was shown that 5-bromo-4-chloro-3-indolyl-β-D-galactopyranoside (X-gal) penetrated *Fatp4* −/− skin, where it was cleaved to produce a colored precipitate by endogenous β-galactosidase activity, whereas the skin of *Fatp4* +/+ and *Fatp4* +/− mice was impermeable (Fig. 5 B). The transepidermal water loss (TEWL) of newborn *Fatp4* −/− mice (12.4 ± 1.2 g/hm^2) was increased by a factor of 9 in comparison with wild-type (1.4 ± 0.35 g/hm^2) and heterozygous (1.4 ± 0.37 g/hm^2) littermates (Fig. 5 C). Thus, we concluded that the abnormal epidermal structure of Fatp4-deficient mice was accompanied by a severely compromised epidermal barrier function.

Another typical feature associated with the homozygous mutant genotype was respiratory distress and cyanosis, accompanied by a gaping mouth and exaggerated diaphragmatic contractions. Histological analysis of the lungs of newborn *Fatp4* −/− mice showed a less than normal extension

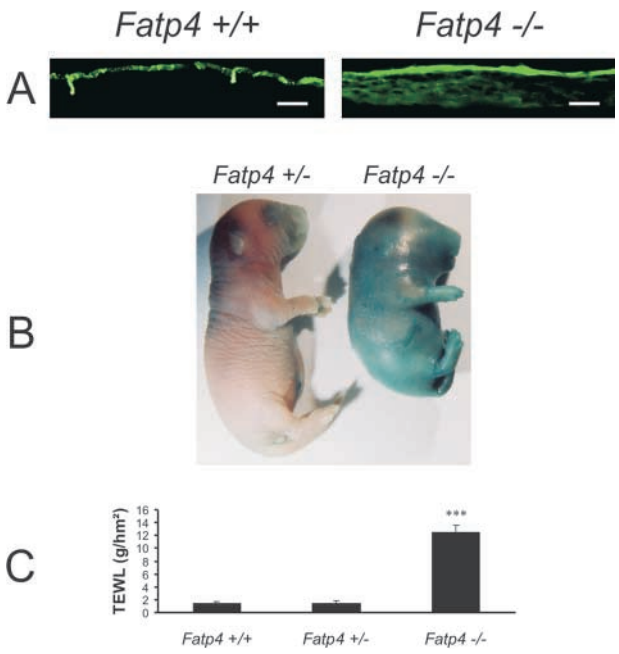

Figure 5. **Disturbed epidermal barrier in *Fatp4* −/− mice.** (A) Diffusion of Lucifer yellow in neonatal mice. The fluorescent dye Lucifer yellow did not pass the upper layers of the stratum corneum in wild-type neonatal mice. In contrast, in *Fatp4* −/− pups, it permeated the entire epidermis. Bars, 50 μm. (B) Access of X-gal to skin of embryonic day 18.5 mice. *Fatp4* +/− epidermis is impermeable for X-gal. In contrast, X-gal permeates Fatp4 −/− skin, where it is cleaved by endogenous β-galactosidase activity to produce a colored precipitate. A *Fatp4* +/− mouse is shown as a control to exclude false-positive staining due to β-galactosidase encoded by the lacZ gene of the mutant *Fatp4* allele. (C) TEWL of dorsal skin, determined in three litters consisting of 10 *Fatp4* +/+, 19 *Fatp4* +/−, and 9 *Fatp4* −/− pups in total. Error bars depict the SEM. ***, $P < 0.001$.

of the alveolae. In addition, the septa were thickened and hypercellular (Fig. 6 A). There were no differences in alveolar cell type II morphology or intra- and extracellular forms of pulmonary surfactant (i. e. lamellar bodies and tubular myelin, respectively) between *Fatp4* +/+ and *Fatp4* −/− mice (Fig. 6 B). All other organs examined by light microscopy appeared normal in *Fatp4* −/− mice, including brain, intestine, liver, kidneys, myocard, thymus, and skeletal muscle (not depicted). No midline defect was detected.

The general capability to move and an adequate reactivity (e. g. squeaking on excitation) indicated no gross abnormality of the nervous system. Light and electron microscopy also revealed no difference between the peripheral nerve structure of *Fatp4* +/+ and *Fatp4* −/− mice. The ultrastructure of the myelin sheaths, in particular, appeared normal in *Fatp4* −/− pups (unpublished data).

Lipid metabolism in *Fatp4* mutant mice

To evaluate whether or not Fatp4 was required for adipose cell development, we subjected embryonic fibroblasts from *Fatp4* +/+ and *Fatp4* −/− embryos to an adipocyte differentiation procedure and verified the results by Oil Red O staining of the neutral lipids. Hereby, no gross differences could be detected between *Fatp4* +/+ and *Fatp4* −/− embryonic fibroblasts concerning their differentiation to fat cells (not depicted).

To examine whether Fatp4 deficiency was accompanied by changes in the respective lipid composition of phosphatidylcholine (PC), sphingomyelin (SPM), phosphatidylethanolamine (PE), phosphatidylserine (PS), and ceramide (CER) in the intestine, liver, lung, brain, dermis, and epidermis, electrospray ionization tandem mass spectrometry (ESI-MS/MS) was performed. Cholesterol (FC), triglycerides (TG), and cholesterylester (CE) were quantified by TLC (Table II). Tissue homogenates of the intestine, liver, lung, brain, and dermis showed no significant differences between *Fatp4* −/− and control *Fatp4* +/+ mice (unpublished data). However, the epidermis of *Fatp4* −/− mice revealed a reduced molar content of PC, PE, and CE, whereas FC and total CERs were increased compared with wild-type littermates (16 and 81%, respectively; Table II, top). Moreover, detailed analysis of the epidermal CER species profile demonstrated that *Fatp4* −/− mice were characterized by a significantly lower proportion of very long chain fatty acids (C26:0 and C26:0-OH) and an increased proportion of fatty acids with <26 carbon atoms (74 ± 2% for *Fatp4* −/− to 36 ± 3% for *Fatp4* +/+; Table II, bottom). A similar shift to shorter chain length was observed for the PC and PS fractions, whereas the species profile of PE and SPM revealed a relative increase of longer fatty acid substitutes (Table III). The SPM profile shift was accompanied by a reduction of the short chain SPM species containing hydroxyl fatty acids (*Fatp4* −/− mice, 28 ± 3%; wild-type littermates, 42 ± 2%). A further difference in the epidermal lipid species composition between *Fatp4* −/− and *Fatp4* +/+

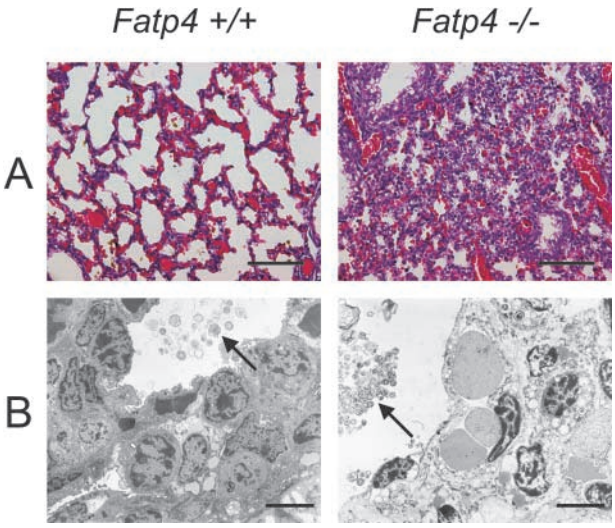

Figure 6. **Lungs of newborn *Fatp4* −/− mice and *Fatp4* +/+ control littermates.** (A) Severe atelectasis of the lung in *Fatp4* mutant mice. *Fatp4* −/− lungs, stained with hematoxylin/eosin, exhibit a reduced extension of the alveolae and an increase in width of the cellular alveolar septae. Bars, 100 μm. (B) Ultrastructural analysis of type II alveolar cells and alveolar surfactant in Fatp4-deficient mice (ruthenium tetroxide fixation). Lung tissue was obtained immediately after birth and prepared for EM. Extracellular forms of surfactant, which can be detected in both *Fatp4* +/+ and *Fatp4* −/− mice without distinction between genotypes, are marked by arrows. Bars, 5 μm.

Table II. **Lipid composition of *Fatp4* +/+ and *Fatp4* −/− epidermis**

Genotype		PC	SPM	PE	PS	CER	FC	TG	CE
		(%)	(%)	(%)	(%)	(%)	(%)	(%)	(%)
Fatp4 +/+	Mean	22.7	4.20	8.3	7.8	1.35	44.1	2.28	9.2
	SD	3.6	0.69	1.2	0.8	0.24	3.3	1.08	2.4
Fatp4 −/−	Mean	19.1*	4.21	6.0***	7.7	2.45***	51.1**	2.86	6.5*
	SD	4.0	0.98	1.1	1.2	0.88	5.4	0.52	3.0

Ceramide

Genotype		C16:0	C18:1	C18:0	C20:0	C22:0	C24:1	C24:0	C26:0	C26:0-OH	Sat.	Unsat.	<C26	≥C26
		(%)	(%)	(%)	(%)	(%)	(%)	(%)	(%)	(%)	(%)	(%)	(%)	(%)
Fatp4 +/+	Mean	7.0	1.1	1.3	1.2	2.8	3.1	17.8	44.8	19.1	95	5	36	64
	SD	1.0	0.1	0.2	0.2	0.3	0.4	0.7	2.0	1.3	1	1	3	3
Fatp4 −/−	Mean	9.6***	1.7*	3.9***	2.7***	6.4***	9.8***	36.7***	13.5***	12.5***	87***	13***	74***	26***
	SD	0.7	0.6	0.7	0.3	0.5	0.5	2.7	2.1	0.6	1	1	2	2

The lipid composition of epidermis is presented as mol percentages for PC, SPM, PE, PS, and CER (quantified by ESI-MS/MS), and for FC, TG, and CE (analyzed by TLC; top). The mol percentages of the saturated and unsaturated lipid species as well as the proportion of species above and below a certain number of carbon atoms in the fatty acid moiety are calculated for CER (bottom). The displayed values are mean ± SD of each 12 *Fatp4* +/+ and 12 *Fatp4* −/− mice analyzed in two independent experiments. Significantly different *Fatp4* +/+ versus *Fatp4* −/−: *, $P < 0.05$; **, $P < 0.01$; ***, $P < 0.001$.

mice was an increased content of the unsaturated CER species in the absence of Fatp4 (13 ± 1% for *Fatp4* −/− to 5 ± 1% for *Fatp4* +/+).

Discussion

It is well established that one stabilizing factor of the epidermal barrier is the arrangement of intra- and extracellular lipid accumulations in the stratum granulosum and the stratum corneum. Aside from FC and fatty acids, CERs constitute the specific lamellar structures of these accumulations and serve as key protectors against environmental offenses and transcutaneous water loss. The essential fatty acid linoleic acid is known to constitute an important component of epidermal CER 1. Insufficient dietary supply or malabsorption leads to ichthyosiform dermatitis, which is characterized by an impaired epidermal proliferation and differentiation. Perturbance of linoleic acid metabolism may also play a role in the pathogenesis of such common skin diseases as atopic dermatitis or psoriasis vulgaris (for review see Wright, 1991). In addition to epidermal sphingolipid biosynthesis, the processing of intracellular lipids and the process of their extrusion into the intercellular space are further essential steps in establishing a functional epidermal lipid barrier. This has also been seen in various gene knockout mouse models, in which distinct defects in the metabolic pathways involved in epidermal barrier formation have been demonstrated. All mice of this type die within the early neonatal period, and (1) the skin-specific disruption of the *Pig-a* gene—an X-linked gene essential for GPI-anchor biosynthesis—reveals a wrinkled and scaly skin with a tightly packed and thickened epidermal horny layer. The intercellular space is narrow and contains many small "vesicles" (Tarutani et al., 1997). In this paper, it has also been shown that GIP-anchored proteins are involved in lipid (CER) transport into the extracellular space of the stratum corneum; (2) mice lacking transglutaminase 1 (keratinocyte transglutaminase) reveal a deficient cross-linking of cell envelope components, associated with an impaired development and maturation of the stratum corneum (Matsuki et al., 1998); and (3) deletion of the Krueppel-like factor 4 (*Klf4*) leads to transcriptional up-regulation of specific essential cornified envelope proteins (Sprr2a, Rptn, Planh2), thereby altering the structural scaffold on which the lipid lamellae are organized (Segre et al., 1999).

All of the gene knockout mouse models described so far have shown a perturbation of the later stages of epidermal differentiation that are essential in establishing an intact transport barrier and forming the cornified envelope. More recently, it has also been shown that in claudin-1–deficient mice, the epidermal barrier is severely impaired, although the layer organization of keratinocytes appears normal (Furuse et al., 2002; for review see Tsuruta et al., 2002). Here, the normal claudin-based tight junction system (zonula occludens) appears leaky. Due to the increased skin permeability, the animals die within the first postnatal day, thus demonstrating that tight junctions represent another key factor of the epidermal barrier and liquid retention.

The results of the present paper are obviously important in the concept that the arrangement of the lipids in the epidermis plays a central role in the tight sealing of the skin. Apparently, both immunolocalizations of Fatp4 in endomembranes and in the plasma membrane, as also shown in the present paper, would be in good agreement with the location and function of a fatty acid transporter (compare with Stahl et al., 1999). A general immunolocalization of Fatp4 on the apical side of mature enterocytes has been reported by Stahl et al. (1999), whereas a strict membrane association has been shown for Fatp1 in transfected mouse NIH 3T3 and hamster Cos7 cells (Lewis et al., 2001).

The disruption of the *Fatp4* gene leads to neonatal mortality in mice, with marked phenotypic alterations, indicative of a vital role of Fatp4 in epidermal development. *Fatp4* −/− mice display a significant thickening of the epidermis with a "too-small-for-size" volume and a more compact dermis, accompanied by a smaller number of pilo-sebaceous structures and a reduced amount of fatty tissue in the hypodermis. Consequently, these mice appear to be caught within their own armor of skin, and general movements

Table III. **Epidermal lipid analysis of *Fatp4* +/+ and *Fatp4* −/− mice by ESI-MS/MS**

Phosphatidylcholine

Genotype		Sat.	Unsat.	<C40	≥C40
		(%)	(%)	(%)	(%)
Fatp4 +/+	Mean	14	86	86	14
	SD	1	1	1	1
Fatp4 −/−	Mean	18***	82***	91***	9***
	SD	1	1	2	2

Phosphatidylethanolamine

Genotype		Sat.	Unsat.	<C38	≥C38
		(%)	(%)	(%)	(%)
Fatp4 +/+	Mean	3.6	96	85	15
	SD	0.2	0	2	2
Fatp4 −/−	Mean	4.4	96	79**	21**
	SD	0.6	1	4	4

Phosphatidylserine

Genotype		Sat.	Unsat.	<C42	≥C42
		(%)	(%)	(%)	(%)
Fatp4 +/+	Mean	5.1	95	79	21
	SD	0.5	0	2	2
Fatp4 −/−	Mean	5.4	95	86***	14***
	SD	1.0	1	1	1

Sphingomyelin

Genotype		Sat.	Unsat.	<C22	≥C22
		(%)	(%)	(%)	(%)
Fatp4 +/+	Mean	91	8.8	76	24
	SD	1	0.9	2	2
Fatp4 −/−	Mean	90	9.5	65***	35***
	SD	0	0.5	2	2

The percentage of saturated and unsaturated lipid species as well as the proportion of species above and below a certain number of carbon atoms in the fatty acid moiety are calculated for PC, PE, PS, and SPM. The displayed values are mean ± SD of each 12 *Fatp4* +/+ and 12 *Fatp4* −/− mice analyzed in two independent experiments. Significantly different *Fatp4* +/+ versus *Fatp4* −/−: **, $P < 0.01$; ***, $P < 0.001$.

seem difficult. Moreover, in some of the *Fatp4* −/− pups, the intraabdominal pressure resulting from the embryonal development of the internal organs apparently forces the intestine to herniate out of the abdominal cavity. The rigid skin consistency most likely also contributes to the mechanical incapability of the lungs to ventilate sufficiently. Morphologically, this is accompanied by hyperproliferation of alveolar septae. Although the lung lipid composition and the formation of lamellar bodies by type II alveolar cells appear normal, we cannot definitively exclude a more subtle lipid disturbance as an explanation for the observed respiratory failure. Clearly, before death the animals experience respiratory distress and cyanosis. Another possible lethal factor might be progressive dehydration due to an impairment of the skin barrier function.

The phenotype described here resembles the human lethal tight skin contracture syndrome (synonymously described as hyperkeratosis-contracture syndrome, lethal restrictive dermopathy, fetal hypokinesia sequence due to restrictive dermopathy; MIM 275210; Holbrook et al., 1987; Sergi et al., 2001). Both in human restrictive dermopathy and in *Fatp4* −/− mice, the dermal–epidermal junction was remarkably flat and the pilo-sebaceous structures were significantly reduced in number and were underdeveloped. The dermis of *Fatp4* −/− mice appeared compact, comparable to the finding in the infant with restrictive dermopathy described by Sergi et al. (2001). In parallel to this case, but in contrast to the infants described by Holbrook et al. (1987), the amount of subcutaneous fat in *Fatp4* −/− mice was not increased. It is unclear whether this difference is a consequence of different pathogenetic mechanisms underlying the reported cases of human restrictive dermopathy and the disorder observed in *Fatp4* −/− mice, or whether it reflects an unspecific difference due to variable degrees of maturation. The similarity between human restrictive dermopathy and the phenotype of *Fatp4* −/− mice remarkably extends to the additional expression of the genes encoding keratins 6 and 16 in both species (Holbrook et al., 1987).

The murine *Fatp4* gene is localized on chromosome 2 band B, which is syntenic to the human chromosome 9 band q34, the location of the human *FATP4* gene. Database searches for mouse (Mouse Genome Informatics database; http://www.informatics.jax.org) and man (Online Mendelian Inheritance in Man; http://www.ncbi.nlm.nih.gov/omim) revealed a number of abnormalities associated with these regions, but no disorder that resembles the phenotype of our *Fatp4* −/− mice. Analysis of cases with lethal restrictive dermopathy will reveal whether the human disease is associated with a mutation in the *FATP4* gene.

Another group of inherited human diseases sharing common features with the phenotype of *Fatp4* −/− mice are the ichthyoses, which are characterized by an excessive amount of scales on the skin, resembling the scales of a fish. The ichthyoses are a complex and variable group of genodermatoses. They are histologically characterized by a markedly thickened stratum corneum (hyperkeratosis) associated with either hypergranulosis or hypogranulosis. In harlequin ichthyosis (MIM number 242500), a particularly severe form, the entire body is covered with thick, horny plaques that are separated by fissures. The harlequin ichthyosis mouse mutation described by Sundberg et al. (1997) leads to thick skin due to formation of compact scales, histologically characterized by massive hyperplasia of the interfollicular epidermis and root sheaths of follicles. Homozygous mutant mice die between 9 and 12 d of age, but are not distinguishable from healthy littermates until 5 d of age, the time when hair fibers emerge from follicles. Thus, both the morphology of these mice and the time of onset of the alterations differ considerably from the phenotype of *Fatp4* −/− mice. However, a possible relation between the phenotype of *Fatp4* −/− mice and human epidermal abnormalities other than restrictive dermopathy cannot be excluded, particularly because the correlation between genotype and phenotype can differ significantly between the two species mouse and man.

During mouse development, maturation of the epidermis as a keratinized stratified squamous epithelium begins at embryonic day 15 (Byrne et al., 1994). The unique appearance and the histological features of the *Fatp4* −/− pups have not been detected before embryonic day 16.5. Due to the re-

strictive dermopathy, the overall size and weight of *Fatp4* −/− mice are reduced, compatible with late intrauterine growth retardation.

As the neurological status of *Fatp4* −/− mice has not been affected and all other organs have appeared morphologically normal, even tissues known for a constitutively high concentration of Fatp4 such as intestine, heart, liver, adipose tissue, and brain, we conclude that the skin is the focus of the metabolic and lethal disorder observed in neonatal *Fatp4* −/− mice. More specifically, it seems to be the lack of Fatp4 in the stratum spinosum and stratum granulosum that leads to the observed phenotype, accompanied by hyperproliferation of keratinocytes and hyperkeratosis.

Because the defective mutant phenotype described here shows similarities with disorders of epidermal lipid metabolism (Elias and Brown, 1978; Schmuth et al., 2000), the lipid composition of the epidermis of *Fapt4* −/− and wild-type mice has been carefully compared. Together with free fatty acids, CERs and FC are the most abundant lipids in the stratum corneum (Elias, 1983). The hyperkeratosis in *Fatp4* −/− mice is characterized by an increase in the relative amounts of the latter two kinds of lipids and, when compared with wild-type mice, the change has been most remarkable for the CER fraction (81% more epidermal CERs compared with *Fatp4* +/+ mice). Most importantly, a significant reduction in the saturated very long chain fatty acid substitutes, C26:0 and C26:0-OH, has also been detected, and the proportion of shorter fatty acid substitutes (<C26) within the CER fraction has increased.

These described findings substantiate the proposed intrinsic acyl-CoA synthetase activity of Fatp4 with its preference for very long chain fatty acids (Herrmann et al., 2001). That Fatp4 deficiency specifically affects the epidermal development could be due to the selective metabolic requirements of keratinocytes that are not adequately compensated by other enzymes or other members of the Fatp family. Moreover, the observed changes in the fatty acid composition of other lipid classes indicate that the effect of Fatp4 deficiency is not only limited to CERs. Although a shift from longer to shorter chain lengths has also been noted for both the PC and PS species of *Fatp4* −/− mice, SPM and PE species show an inverse behavior. Thus, the role of Fatp4 in the control of acylation reactions may be more complex, and further studies are clearly necessary to define the exact mode of action.

CERs with long and very long chain fatty acid substitutes are essential for the molecular organization of stratum corneum lipids, which eventually constitute the lamellar membranous structures of the skin (Bouwstra et al., 2001). In *Fatp4* −/− mice, CERs not only show an altered fatty acid chain length profile, but also show a significant increase in unsaturated fatty acids. It is tempting to speculate that these alterations may result in changes of the stability and fluidity of the membranous structures in the stratum corneum intercellular space and therefore account for the observed epidermal abnormalities (Norlen, 2001). Obviously, impairment of the epidermal lipid barrier may be caused by a disturbance of the intracellular CER biosynthesis and processing, or by a disturbed extracellular arrangement of the lipid aggregates, or by both effects. For the correct assembly of the extruded epidermal lipids, the attachment of glucosylceramides to proteins of the cornified envelope has been proposed (Doering et al., 1999a,b). As discussed earlier in this section, the other stabilizing factor of the skin barrier is the system of claudin-based tight junctions prominently present in the stratum granulosum (Morita et al., 1999; Pummi et al., 2001; Brandner et al., 2002; Furuse et al., 2002; Langbein et al., 2002). Consequently, claudin-1–deficient mice reveal a severely impaired epidermal barrier leading to dehydration and neonatal death. Therefore, it is most likely that both systems, the lipid lamellae abundant in the stratum corneum and the tight junctions of the stratum granulosum, are required to provide optimally efficient sealing and liquid retention in the mammalian epidermis.

In conjunction with the abnormal lipid composition, the epidermis of *Fatp4* −/− mice has shown an increased number of cell layers in the stratum spinosum and a significantly reduced size of keratohyalin granules in the stratum granulosum. Whether the disturbed terminal differentiation of the epidermis reflects an unspecific reaction to the defective epidermal barrier or whether it is directly caused by an altered epidermal lipid composition remains to be elucidated. Indeed, in addition to their structural role in the epidermis, CERs are also involved in various signaling pathways that control differentiation and proliferation (Huwiler et al., 2000). However, possible contributions of impaired lipid signaling to the pathophysiology of *Fatp4* −/− mice remain presently elusive.

With the exception of the skin alterations and the (secondary) reduced capacity of the alveolae to distend, no other significant abnormalities have been noted in *Fatp4*-null mice, including morphology, adipocyte differentiation, and organ lipid composition. This suggests that Fatp4-mediated processes are either highly tissue-specific, or that its functional role can be compensated by other proteins in most tissues, except the skin. However, the rapid neonatal death of *Fatp4* −/− mice may have obscured other Fatp4 functions, e.g., intestinal fatty acid absorption. Further studies with conditional *Fatp4* alleles and suitable *Cre*-expressing mice should permit exploration of such possibilities.

Materials and methods

Generation of *Fatp4* mutant mice

Lambda phage clones containing the *Fatp4* gene were isolated from a mouse strain 129/Ola genomic library as described previously (Herrmann et al., 2001). A restriction fragment containing the region from nt 1–7359 of the *Fatp4* genomic sequence (GenBank/EMBL/DDBJ accession no. AJ276492) was subcloned into pBluescript® II (Stratagene). To generate a targeting construct, by ET recombination (Zhang et al., 2000) a 7172-bp cassette was inserted into intron 2 between nt positions 3193 and 3194, and a 117-bp cassette was inserted into intron 3 replacing nt 3814–3817 (Fig. 1 A). The targeting vector was linearized with NotI and electroporated into E14–1 embryonic stem (ES) cells. DNA from neomycin-resistant ES cell colonies was screened by Southern analysis using 5′ and 3′ probes flanking the recombination arms (Fig. 1 B). Six homologous recombinants were identified of 17 analyzed. ES cells from two of the six positive clones were injected into C57BL/6 blastocysts to generate chimeric mice, which were mated with C57BL/6 females. F1 heterozygotes were intercrossed to generate *Fatp4* −/− mice. Animals derived from two ES cell clones were analyzed separately and were shown to be phenotypically identical. Adult and newborn mice were genotyped by using three PCR primers (mmF4-In2f, 5′-CTGTTTGAAAGGTGCTGTGC-3′; mmF4-pUX4r, 5′-AGTCCTCTTCACATCCATGC-3′; mmF4-wtIn3r, 5′-TCTGGTGCCGAGACTCATAC-3′) under the following conditions: 0.75 mM $MgCl_2$, 35 cycles of 94°C for 30 s, 55°C for 30 s, and 72°C for 1 min. The mutant band was 830 bp; the wild-type band was 1064 bp (Fig. 1 C).

To convert the targeted allele into a mutant *Fatp4* allele structurally lacking an essential part of the *Fatp4* gene, mice carrying the mutant *Fatp4* allele (named *Fatp4-K*) were crossed with *PGK-Cre* transgenic mice (provided by Klas Kullander (AstraZeneca, Mölndal, Sweden) and Ruediger Klein (Max Planck Institute of Neurobiology, Martinsried, Germany) exhibiting ubiquitous *Cre* expression (Schwenk et al., 1995). In the resulting double-mutant mice, the region between the two loxP sites containing exon 3 was excised, resulting in a defective *Fatp4* allele (named *Fatp4-KO*) still containing the selection cassette in intron 2, but in addition lacking exon 3 (Fig. 1 A). Offspring homozygous for the *Fatp4-KO* or *Fatp4-K* alleles were analyzed for morphological differences and were both found to be identical.

Fatp4 expression was controlled by Northern blot analysis. 20 μg total RNA prepared from total intestine was electrophoresed in a 1.2% agarose gel containing 0.66 M formaldehyde, transferred onto nylon membrane, and subjected to hybridization as described previously (Herrmann et al., 2001). All mouse procedures were in compliance with the guidelines of the institutional animal care and use committees and in accordance with governmental guidelines.

Antibodies

Primary pAbs against mouse Fatp4 were generated using the synthetic peptide APKHLPSHPDKGFTD to which a cysteine residue had been added before coupling to keyhole limpet hemocyanin. The antiserum was produced by injection of guinea pigs (Peptide Specialty Laboratories). For comparison, antibodies used in immunohistochemistry were as follows: (1) rabbit antibodies to occludin, claudin 1, protein ZO-1 (all from Zytomed), to keratins K16 (gift of Dr. P. Coulombe, Johns Hopkins University School of Medicine, Baltimore, MD) and K10 (gift of Dr. D. Roop, Baylor College, Houston, TX), to periplakin and loricrin (both antisera were gifts of Dr. D. Hohl, Hopital de Beaumont, Lausanne, Switzerland); (2) guinea pig antibodies against keratins K2e, K5 and K14 (all from Progen Biotechnik); and (3) mouse antibodies to keratin K6 (clone KA12; Progen Biotechnik), filaggrin (mouse ascites; from Quartett Co., or from Paesel & Lorei) and to transglutaminase 1, TG-1 (Cell Systems).

The secondary antibodies used for indirect immunofluorescence were goat anti–guinea pig, anti–rabbit or anti–mouse immunoglobulins coupled to Alexa® 568 (dilution of 1:200; Molecular Probes, Inc.). For ECL, HRP-coupled anti–guinea pig IgGs (H+L; Dianova) were used at a dilution of 1:10,000. Immunoblots were performed as described previously (Coe et al., 1999).

Histological and electron microscopic analysis

Newborn mice and fetal mice of different developmental stages were killed, fixed in 4% neutral formaldehyde solution, and embedded in paraffin. Sections were cut at 3 μm and stained with hematoxylin/eosin, Masson's trichrome, periodic acid Schiff, Verhoeff van Gieson, Oil Red O, and cresyl violet-Luxol fast blue, respectively. EM was performed essentially as described previously (Hou et al., 1991; Elhalwagi et al., 1999).

Skeleton preparations

Skin and internal organs were carefully removed from killed newborn mice. Carcasses were fixed in 95% ethanol for 4 d and in acetone for 3 d, and were then stained with 0.015% Alcian blue/0.005% Alizarin red sodium sulfate/5% acetic acid (Sigma-Aldrich) for 7–10 d. The samples were cleared in 2% KOH for 2–3 d and then in 1% KOH – 20% glycerol for 2–7 d. Skeletons were subsequently stored in 50, 80, and 100% glycerol and photographed.

Immunofluorescence microscopy

Indirect immunofluorescence microscopy was done using various protocols in parallel. The standard protocol was essentially as described elsewhere for several membrane-associated proteins (Schmidt et al., 1997; Langbein et al., 2002). In brief, after rinsing with PBS, cryostat sections of shock-frozen tissues of mouse back skin, snout, and pad were fixed in acetone (5 min at −20°C), permeabilized with 0.1% Triton X-100/PBS for 2 min, and blocked with 5% normal goat serum in PBS. Primary antibodies were applied for 1 h, slides were rinsed in PBS, secondary antibodies were added for 30 min, and specimens were again washed in PBS, rinsed in ethanol, dried, and mounted. For Fatp4 immunostaining, to prevent possible losses of membrane-bound or soluble antigens from cryostat sections during the immunolocalization procedures, various alternative fixation and incubation protocols were used (protocols 2 and 3; see Schmidt et al., 1997). In brief, in procedure 2, the standard protocol was modified to avoid the use of detergent in any of the buffers, and all antibody incubations were shortened to 15 min and the washing steps to 3 min. In protocol 3, the initial fixation was in freshly prepared, 2% formaldehyde in PBS (15 min at RT), followed by rinsing in PBS, blocking in 50 mM NH_4Cl (freshly prepared, 10 min at RT), and final rinsing in PBS. Control immunostaining reactions were as follows: (1) using the secondary antibodies only; (2) using the Fatp4 antiserum after absorption with the synthetic peptide used for immunization; and (3) using a keratin K14–specific guinea pig antiserum instead of the Fatp4 antiserum. Furthermore, the suitability of the Fatp4 antibodies was controlled in cryosections through small intestine of *Fatp4* +/+ and −/− mice, in which a prominent apical staining was apparent in the enterocytes of wild-type mice, but not of *Fatp4* −/− mice (Stahl et al., 1999). Visualization and documentation were performed with a photomicroscope (Axiophot II; Carl Zeiss MicroImaging, Inc.).

Skin permeability assay

The diffusion of 1 mM Lucifer yellow in Ringer's solution (pH 7.4) at 37°C was analyzed in neonatal *Fatp4* −/− and control mice essentially as described earlier (Matsuki et al., 1998). The frozen skin samples were sliced at a thickness of 5 μm. The sections were analyzed by fluorescence microscopy. In addition, barrier-dependent access of X-gal to untreated skin was examined in embryonic day 18.5 *Fatp4* +/+, *Fatp4* +/−, and *Fatp4* −/− mice as described previously (Hardman et al., 1998).

Measurement of TEWL

The TEWL from dorsal skin of neonatal mice was determined as described previously (Matsuki et al., 1998) by using a transepidermal water loss instrument (TEWAMETER® TM 210; Courage and Khazaka Electronic) according to the manufacturer's instructions. The instrument is an open chamber system with two humidity and temperature sensor pairs that measure the water evaporation gradient at the surface of the skin. Measurements were performed with a special probe for small sample areas.

Adipocyte differentiation of embryonic fibroblast cells

Preparation of primary embryonic fibroblasts and induction of adipogenic differentiation were performed according to methods described previously (Tanaka et al., 1997). Embryonic fibroblast cells from *Fatp4* +/+ and *Fatp4* −/− day 13.5 embryos were cultured in the presence of standard differentiation-induction medium, containing 0.5 mM 3-isobutyl-1-methylxanthine, 0.25 μM dexamethasone, 1 μg/ml insulin, 5 μg/ml ciglitazone, and 10% FBS in DME. After 10 d of differentiation, cells were observed by light microscopy with Oil Red O staining.

Lipid analysis

Epidermis and dermis were separated with forceps after incubation of skin pieces in 25 U/ml dispase for 16–24 h at 4°C. Phospholipids in intestine, liver, lung, brain, dermis, and epidermis were quantified by ESI-MS/MS according to the principles described by Brugger et al. (1997). In brief, tissue homogenates were extracted according to the protocol of Bligh and Dyer (1959). Prior lipid extraction, not naturally occurring lipid species were added as internal standards: 1,2-dimyristoyl-sn-glycero-3-phosphocholine (PC 28:0) and 1,2-dibehenoyl-*sn*-glycero-3-phosphocholine (PC 44:0) for PC and SPM; 1,2-dimyristoyl-*sn*-glycero-3-phosphoethanolamine (PE 28:0) for PE; and 1,2-dimyristoyl-*sn*-glycero-3-phosphoserine (PS 28:0) for PS. Lipid extracts were characterized by ESI-MS/MS using an HPLC system (Waters® Alliance separations module 2790; Milford) coupled to a triple quadrupol mass spectrometer (Quattro Ultima; Micromass). Sphingosine backbone–containing CERs were analyzed similar to the previously described methodology (Liebisch et al., 1999) using *N*-heptanoyl-sphingosine (CER 17:0) as internal standard. Due to an isotope overlap of PC and SPM species, intensities were corrected by theoretically calculated isotope pattern. Neutral lipids were determined as described previously (Klucken et al., 2000) by TLC.

Statistical methods

Data are shown as mean ± SD. Measurements in *Fatp4* +/+, *Fatp4* +/−, and *Fatp4* −/− mice, respectively, were compared by *t* test.

We are grateful to Dr. C. Sergi for histological evaluation of the skin morphology. We thank A. Peter, P. Hornsberger, G. Schmidt, S. Kaden, S. Praetzel, K. Vintersten, and D. Mueller for their expert technical assistance; Drs. K. Kullander and R. Klein for providing the *PGK-Cre* transgenic mice; Dr. H.-P. Schmitt for neuropathological assessment of central nervous system sections; Drs. N. Schuerer and B. Melnik for helpful advice regarding the analysis of the skin phenotype; and Dr. C. Reininger for critical review of the manuscript.

This work was supported by grants from the Deutsche Forschungsgemeinschaft (STR 216/11-1) and the Dietmar-Hopp-Foundation to W. Stremmel, and the Faculty of Medicine, University of Heidelberg, to T. Herrmann (junior scientist grants 239/2000, 68/2001, and 120/2002).

Submitted: 15 July 2002
Revised: 1 May 2003
Accepted: 5 May 2003

References

Berger, J., C. Truppe, H. Neumann, and S. Forss-Petter. 1998. A novel relative of the very-long-chain acyl-CoA synthetase and fatty acid transporter protein genes with a distinct expression pattern. *Biochem. Biophys. Res. Commun.* 247:255–260.

Bligh, E.G., and W.J. Dyer. 1959. A rapid method of total lipid extraction and purification. *Can. J. Biochem. Physiol.* 37:911–917.

Bouwstra, J., G. Pilgram, G. Gooris, H. Koerten, and M. Ponec. 2001. New aspects of the skin barrier organization. *Skin Pharmacol. Appl. Skin Physiol.* 14(Suppl 1):52–62.

Brandner, J.M., S. Kief, C. Grund, M. Rendl, P. Houdek, C. Kuhn, E. Tschachler, W.W. Franke, and I. Moll. 2002. Organization and formation of the tight junction system in human epidermis and cultured keratinocytes. *Eur. J. Cell Biol.* 81:253–263.

Brugger, B., G. Erben, R. Sandhoff, F.T. Wieland, and W.D. Lehmann. 1997. Quantitative analysis of biological membrane lipids at the low picomole level by nano-electrospray ionization tandem mass spectrometry. *Proc. Natl. Acad. Sci. USA.* 94:2339–2344.

Byrne, C., M. Tainsky, and E. Fuchs. 1994. Programming gene expression in developing epidermis. *Development.* 120:2369–2383.

Coe, N.R., A.J. Smith, B.I. Frohnert, P.A. Watkins, and D.A. Bernlohr. 1999. The fatty acid transport protein (FATP1) is a very long chain acyl-CoA synthetase. *J. Biol. Chem.* 274:36300–36304.

Doering, T., W.M. Holleran, A. Potratz, G. Vielhaber, P.M. Elias, K. Suzuki, and K. Sandhoff. 1999a. Sphingolipid activator proteins are required for epidermal permeability barrier formation. *J. Biol. Chem.* 274:11038–11045.

Doering, T., R.L. Proia, and K. Sandhoff. 1999b. Accumulation of protein-bound epidermal glucosylceramides in beta-glucocerebrosidase deficient type 2 Gaucher mice. *FEBS Lett.* 447:167–170.

Elhalwagi, B.M., M. Zhang, M. Ikegami, H.S. Iwamoto, R.E. Morris, M.L. Miller, K. Dienger, and F.X. McCormack. 1999. Normal surfactant pool sizes and inhibition-resistant surfactant from mice that overexpress surfactant protein A. *Am. J. Respir. Cell Mol. Biol.* 21:380–387.

Elias, P.M. 1983. Epidermal lipids, barrier function and desquamation. *J. Invest. Dermatol.* 80:44–49.

Elias, P.M., and B.E. Brown. 1978. The mammalian cutaneous permeability barrier. *Lab. Invest.* 39:574–583.

Furuse, M., M. Hata, K. Furuse, Y. Yoshida, A. Haratake, Y. Sugitani, T. Noda, A. Kubo, and S. Tsukita. 2002. Claudin-based tight junctions are crucial for the mammalian epidermal barrier: a lesson from claudin-1–deficient mice. *J. Cell Biol.* 156:1099–1111.

Gimeno, R.E., A.M. Ortegon, S. Patel, S. Punreddy, P. Ge, Y. Sun, H.F. Lodish, and A. Stahl. 2003. Characterization of a heart-specific fatty acid transport protein. *J. Biol. Chem.* 278:16039–16044. First published on January 28, 2003; 10.1074/jbc.M211412200.

Hardman, M.J., S. Paraskevi, D.N. Banbury, and C. Byrne. 1998. Patterned acquisition of skin barrier function during development. *Development.* 125:1541–1552.

Herrmann, T., F. Buchkremer, I. Gosch, A.M. Hall, D.A. Bernlohr, and W. Stremmel. 2001. Mouse fatty acid transport protein 4 (FATP4): Characterization of the gene and functional assessment as a very long chain acyl-CoA synthetase. *Gene.* 270:31–40.

Hirsch, D., A. Stahl, and H.F. Lodish. 1998. A family of fatty acid transporters conserved from mycobacterium to man. *Proc. Natl. Acad. Sci. USA.* 95: 8625–8629.

Holbrook, K.A., B.A. Dale, D.R. Witt, M.R. Hayden, and H.V. Toriello. 1987. Arrested epidermal morphogenesis in three newborn infants with a fatal genetic disorder (restrictive dermopathy). *J. Invest. Dermatol.* 88:330–339.

Hou, S.Y.E., A.K. Mitra, S.H. White, G.K. Menon, R. Ghadially, and P.M. Elias. 1991. Membrane structures in normal and essential fatty acid-deficient stratum corneum: characterization by ruthenium tetroxide staining and x-ray diffraction. *J. Invest. Dermatol.* 96:215–223.

Huwiler, A., T. Kolter, J. Pfeilschifter, and K. Sandhoff. 2000. Physiology and pathophysiology of sphingolipid metabolism and signaling. *Biochim. Biophys. Acta.* 1485:63–99.

Klucken, J., C. Buechler, E. Orso, W.E. Kaminski, M. Porsch-Ozcurumez, G. Liebisch, M. Kapinsky, W. Diederich, W. Drobnik, M. Dean, et al. 2000. ABCG1 (ABC8), the human homolog of the Drosophila white gene, is a regulator of macrophage cholesterol and phospholipid transport. *Proc. Natl. Acad. Sci. USA.* 97:817–822.

Langbein, L., C. Grund, C. Kuhn, S. Praetzel, J. Kartenbeck, J. Brandner, I. Moll, and W.W. Franke. 2002. Tight junctions and compositionally related junctional structures in mammalian stratified epithelia and cell cultures derived therefrom. *Eur. J. Cell Biol.* 81:419–435.

Lewis, S.E., L.L. Listenberger, D.S. Ory, and J.E. Schaffer. 2001. Membrane topology of the murine fatty acid transport protein 1. *J. Biol. Chem.* 276: 37042–37050.

Liebisch, G., W. Drobnik, M. Reil, B. Truembach, R. Arnecke, B. Olgemoeller, A. Roscher, and G. Schmitz. 1999. Quantitative measurement of different ceramide species from crude cellular extracts by electrospray ionization tandem mass spectrometry (ESI-MS/MS). *J. Lipid Res.* 40:1539–1546.

Matsuki, M., F. Yamashita, A. Ishida-Yamamoto, K. Yamada, C. Kinoshita, S. Fushiki, E. Ueda, Y. Morishima, K. Tabata, H. Yasuno, et al. 1998. Defective stratum corneum and early neonatal death in mice lacking the gene for transglutaminase 1 (keratinocyte transglutaminase). *Proc. Natl. Acad. Sci. USA.* 95:1044–1049.

Morita, K., M. Furuse, K. Fujimoto, and S. Tsukita. 1999. Claudin multigene family encoding four-transmembrane domain protein components of tight junction strands. *Proc. Natl. Acad. Sci. USA.* 96:511–516.

Norlen, L. 2001. Skin barrier structure and function: the single gel phase model. *J. Invest. Dermatol.* 117:830–836.

Pummi, K., M. Malminen, H. Aho, S.-L. Karvonen, and S. Peltonen. 2001. Epidermal tight junctions: ZO-1 and occludin are expressed in mature, developing, and affected skin and in vitro differentiating keratinocytes. *J. Invest. Dermatol.* 117:1050–1058.

Schaffer, J.E., and H.F. Lodish. 1994. Expression cloning and characterization of a novel adipocyte long chain fatty acid transport protein. *Cell.* 79:427–436.

Schmidt, A., L. Langbein, M. Rode, S. Pratzel, R. Zimbelmann, and W.W. Franke. 1997. Plakophilins 1a and 1b: widespread nuclear proteins recruited in specific epithelial cells as desmosomal plaque components. *Cell Tissue Res.* 29:481–499.

Schmuth, M., M.Q. Man, F. Weber, W. Gao, K.R. Feingold, P. Fritsch, P.M. Elias, and W.M. Holleran. 2000. Permeability barrier disorder in Niemann-Pick disease: sphingomyelin-ceramide processing required for normal barrier homeostasis. *J. Invest. Dermatol.* 115:459–466.

Schwenk, F., U. Baron, and K. Rajewsky. 1995. A cre-transgenic mouse strain for the ubiquitous deletion of loxP-flanked gene segments including deletion in germ cells. *Nucleic Acids Res.* 23:5080–5081.

Segre, J.A., C. Bauer, and E. Fuchs. 1999. Klf4 is a transcription factor required for establishing the barrier function of the skin. *Nat. Genet.* 22:356–360.

Sergi, C., J. Poeschl, M. Graf, and O. Linderkamp. 2001. Restrictive dermopathy: case report, subject review with Kaplan-Meier analysis, and differential diagnosis of the lethal congenital contractural syndromes. *Am. J. Perinatol.* 18:39–47.

Stahl, A., D.J. Hirsch, R.E. Gimeno, S. Punreddy, P. Ge, N. Watson, S. Patel, M. Kotler, A. Raimondi, L.A. Tartaglia, and H.F. Lodish. 1999. Identification of the major intestinal fatty acid transport protein. *Mol. Cell.* 4:299–308.

Steinberg, S.J., S.J. Wang, M.C. McGuinness, and P.A. Watkins. 1999. Human liver-specific very-long-chain acyl-coenzyme A synthetase: cDNA cloning and characterization of a second enzymatically active protein. *Mol. Genet. Metab.* 68:32–42.

Stremmel, W., J. Pohl, A. Ring, and T. Herrmann. 2001. A new concept of cellular uptake and intracellular trafficking of long-chain fatty acids. *Lipids.* 36:981–989.

Sundberg, J.P., D. Boggess, M.E. Hogan, B.A. Sundberg, M.H. Rourk, B. Harris, K. Johnson, R.W. Dunstan, and M.T. Davisson. 1997. Harlequin ichthyosis (ichq): a juvenile lethal mouse mutation with ichthyosiform dermatitis. *Am. J. Pathol.* 151:293–310.

Tanaka, T., N. Yoshida, T. Kishimoto, and S. Akira. 1997. Defective adipocyte differentiation in mice lacking the C/EBPbeta and/or C/EBPdelta gene. *EMBO J.* 16:7432–7443.

Tarutani, M., S. Itami, M. Okabe, M. Ikawa, T. Tezuka, K. Yoshikawa, T. Kinoshita, and J. Takeda. 1997. Tissue-specific knockout of the mouse Pig-a gene reveals important roles for GPI-anchored proteins in skin development. *Proc. Natl. Acad. Sci. USA.* 94:7400–7405.

Tsuruta, D., K.J. Green, S. Getsios, and J.C.R. Jones. 2002. The barrier function of skin: how to keep a tight lid on water loss. *Trends Cell Biol.* 12:355–357.

Wright, S. 1991. Essential fatty acids and the skin. *Br. J. Dermatol.* 125:503–515.

Zhang, Y., J.P.P. Muyrers, G. Testa, and A.F. Stewart. 2000. DNA cloning by homologous recombination in *Escherichia coli*. *Nat. Biotechnol.* 18:1314–1317.